Visual
Abstract

Numerical analysis of reinforced concrete circular columns strengthening with CFRP under concentric and eccentric loadings

Ibrahim S. I. Harba, Abdulkhalik J. Abdulridha, Ahmed A. M. AL-Shaar
Department of Civil Engineering, College of Engineering, Al-Nahrain University, Jadriya, Baghdad, Iraq
Ibrahim.S.Ibrahim@nahrainuniv.edu.iq, https://orcid.org/0000-0002-5651-0654
abdulkhalik.j.abdulridha@nahrainuniv.edu.iq, https://orcid.org/0000-0001-6403-2325
ahmed.a.mustafa@nahrainuniv.edu.iq, https://orcid.org/0000-0001-6614-2990

ABSTRACT. The purpose of this study is to explore the numerical behavior of circular Reinforced Concrete (RC) short columns with different degrees of confinement with Carbon Fiber Reinforced Polymer (CFRP) (0%, 25%, 50%, and 100%) wraps under concentric and eccentric loading. The numerical analysis carried out by using an improved Concrete Damage plasticity (CDP) model implemented in ABAQUS software for finite element (FE) analysis. The FE model simulated a total of twenty-four numerical specimens. The findings were matched to published experimental test results in the literature. The findings of the FE model and the experimental data were good similar. As a consequence, the model was found to be valid. The numerical results shows that as load eccentricity increased, the load carrying capacity of columns decreased for unconfined specimens, whereas the decline in strength for confined specimens becomes limited as the degrees of confinement ratio increased. In addition, increasing the CFRP confinement ratio improves the column's load-bearing capability at the same load eccentricity.

KEYWORDS. Short circular column, Numerical analysis, Plastic-damage model, CFRP, Eccentric load, ABAQUS software.

OPEN ACCESS

INTRODUCTION

Since the last two decades, the impact of strengthening existing reinforced concrete columns (RCC) by fiber reinforced polymer (FRP) systems has been develop into the most preferred systems for retrofitting of RC structures. The FRP materials offer in general high stiffness to weight and strength to weight ratios, also offering significant possible for cost effective and durable lightweight. Using CFRP sheet systems led to a significant improvement in the structural behavior of the RC members [1]. The externally bonded CFRP sheets improved the failure mode and the capacity [2]. Covering the service period of longstanding structures by repairing and reinforcing is expected [3].

The majority of studies focused on the behavior of FRP confined reinforced concrete columns subjected to concentric axial loads, while columns subjected to eccentric loads are not well understood [4, 5]. The increase in strength and ductility of eccentrically loaded FRP confined columns less significant compared with concentrically loaded columns [6]. The FRP wrap

columns will lead to an increase in columns strength and flexural ductility [7]. The strength and ductility were decreased with the increase in load eccentricity for all confined columns [8]. The variation in confinement pressure under eccentric loading across the section differs from stress state caused by concentric loading [9-12]. Several experimental studies have been carried out on eccentrically loaded FRP confined circular columns [11, 13-23] and noncircular columns [9, 24-32], reveals that the confinement effectiveness of circular RCC specimens confined with FRP declines with increasing load eccentricity. However, numerous studies have argued that concrete's shear damage may be efficiently reduced by confining a layer of CFRP sheets, which also changes the column specimen's failure mode from brittle-shear to ductile-flexural [33]. Also, the test results showed that the RCC's lateral displacement was significantly decreased under impact loading after being confined by the CFRP [34]. While the maximum displacement only slightly increases, the load - carrying capacity dramatically increases as the number of CFRP sheet layers increases [35].

The three-dimensional non-linear FE method based on CDP was used to overcome the experimental laboratory obstacles as noted previously [36]. This FE models shows accurate and reasonable method in modeling of confined concrete under non-uniform FRP pressure as compared to others FE models (e.g., [37,38]) due to improved constitutive model of CDP. This improved model [36-37] implemented successfully in ABAQUS for FE analysis of circular and square FRP-confined concrete columns, also composite steel columns confined by FRP under concentric loading [39]. Other researchers utilized this model (e.g., [40-42]) due to the ability of providing reasonable stress-strain responses for FRP-confined concrete under both uniform and non-uniform confinement.

In general, limited available tests in open literature on eccentrically loaded circular short RCC confined with CFRP. It is necessary to understand the effect of confinement efficiency and column section under eccentric loading. The aim of this work is to investigate by improved CDP finite element analysis the axial load capacity degradations of CFRP-confined circular short concrete with different load eccentricity and confinement ratio. The accuracy of numerical results of proposed FE approach will be verified by comparing with available experimental test results in literature [43].

OUTLINE OF EXPERIMENTAL PROGRAM

I n this paper a brief outline is discussed of experimental work presented by Kaiss et al. [43], was used in this investigations to calibrate numerical results and validate its application. The details of chosen column specimens from the experimental test conducted by Kaiss et al. [43] shown in Fig. 1. The schemes of strengthening were chosen according to volumetric ratio of transverse CFRP ties (CFRP ratio=0%, 25%, 50% and 100%) as shown in Fig. 2. The details of mechanical properties for the columns specimens are given in Tab. 1 to Tab. 3.
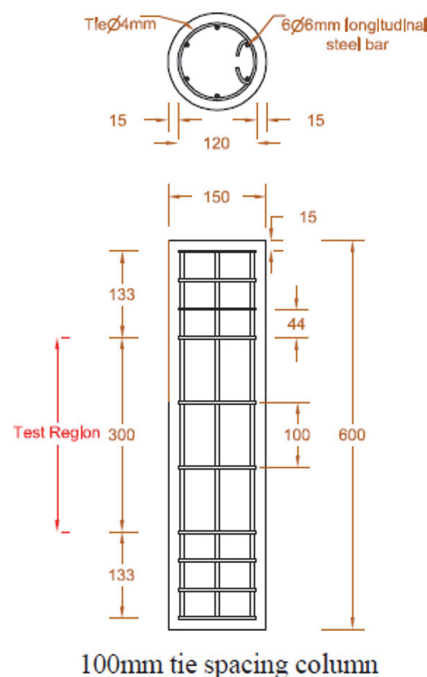

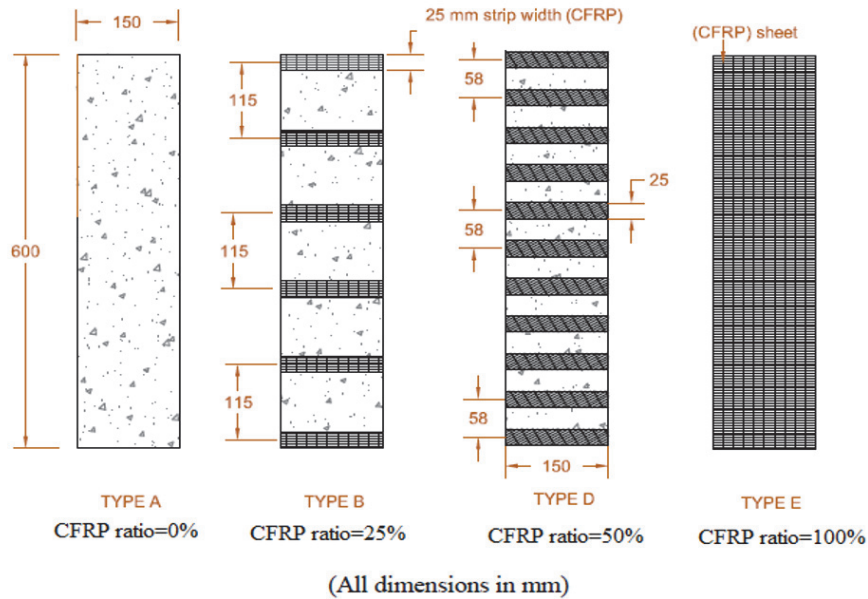Figure 1: Details of column specimens [43]

Figure 2: schemes of CFRP confinement [43].

Areal weight	300g/m² ± 15 g/m²
CFRP thickness (t_f)	0.166 mm
Tensile modulus of elasticity	230 000 N/mm²
Tensile strength	3900 N/mm²
Elongation at break	1.5% (nominal)

Table 1: Mechanical properties of CFRP (Sika Wrap®-300C) [43].

Nominal diameter (mm)	Measured diameter (mm)	Yield strength (MPa)	Ultimate tensile Strength (MPa)	Elongation %
4	4.3	717	751	9.11
6	5.98	513	543	11.66

Table 2: Mechanical properties of steel reinforcement [43].

$f_{c'}$ (MPa)	f_{cu} (MPa)	Splitting tensile strength (MPa)	Modulus of rupture (MPa)	Modulus of elasticity (MPa)
30.12	36.25	2.9	4	28000

Table 3: Mechanical properties for concrete [43].

METHOD AND MATERIAL MODELING

In this research numerical analysis was conducted based on the FE ABAQUS software [44]. Concrete is modelled with solid elements (C3D4R) and reinforcement is modelled using truss elements (T3D2) that are embedded in concrete

solid elements as shown in Fig. 3. The full bond constraint was used to simulate the interaction between reinforcing steel and concrete.

The model of concrete-damaged plasticity was chosen. Both isotropic damage and degradation of the elastic stiffness are represented by the scalar degradation damage parameter $0 \leq D < 1$ to represent isotropic damage and elastic stiffness degradation Lee and Fenves [45] as Eq. (1):

$$\overline{\sigma} = (1- D) \, E_0 : (\varepsilon - \varepsilon^{pl}) \tag{1}$$

Where E_0 is the initial elastic stiffness, $\overline{\sigma}$ is the effective stress, ε is the strain tensor, and ε^{pl} is the plastic strain tensor. More significant damage results from a bigger D. When D is 0, there is no damage to the concrete, and the original elastic stiffness is maintained during unloading. Two variables are specified in Eq. (2) to express damage states in tension and compression, respectively, because tension and compression have different reaction characteristics:

$$D = 1- (1 - D_t) \, (1 - D_c) \tag{2}$$

Where, respectively, $0 \leq D_t < 1$ and $0 \leq D_c < 1$ are tensile and compressive degradation damage responses. According to this theory, two damage factors d_t and d_c are regarded as functions of the plastic strain, temperature, and field variables as Eqs. (3) and (4), are used to describe the deterioration of elastic stiffness:

$$d_c = \mathrm{d_c}(\tilde{\varepsilon}_c^{pl}, \theta, f_i) \tag{3}$$

$$d_t = \mathrm{d_t}(\tilde{\varepsilon}_t^{pl}, \theta, f_i) \tag{4}$$

Where $\tilde{\varepsilon}_c^{pl}$ and $\tilde{\varepsilon}_t^{pl}$ are the comparable plastic strains, θ is the temperature, and f_i are other predetermined field variables. Particularly, the residual concrete compression strength, which is defined as the crushing of concrete, is 20% of compression strength when dc equals 0.9. According to Lubliner et al. [46] as Eqs. (5) to (8), a yield function is provided to more accurately reflect the two distinct behaviors in the tensile area and compressive region:

$$F = \frac{1}{1- \alpha} \, (\, \overline{q} \, - 3\alpha \, \overline{p} \, + \beta(\overline{\varepsilon}^{pl}) < \hat{\overline{\sigma}} \max >) - \overline{\sigma}c \, \left(\overline{\varepsilon}_c^{pl} \right) = 0 \tag{5}$$

$$\alpha = \frac{\left(\dfrac{\sigma b0}{\sigma c0} \right) - 1}{2\left(\dfrac{\sigma b0}{\sigma c0} \right) - 1} \; ; 0 \leq \alpha \leq 0.5 \tag{6}$$

$$\beta = \frac{\sigma c \left(\overline{\varepsilon}_l^{pl} \right)}{\sigma c \left(\overline{\varepsilon}_l^{pl} \right)} (1- \alpha) - (1 + \alpha) \tag{7}$$

$$\gamma = \frac{3(1- Kc)}{2Kc - 1} \tag{8}$$

where $\hat{\overline{\sigma}} \max$ stands for the highest primary effective stress, σ_{bo}/σ_{co} for the ratio of the first equi-axial compressive yield stress to the initial uniaxial compressive yield stress, $\overline{\sigma}t \left(\overline{\varepsilon}_t^{pl} \right)$ stands for the effective tensile cohesion stress, $\overline{\sigma}c \left(\overline{\varepsilon}_c^{pl} \right)$ stands for the effective compressive stress, and K_c stands for the ratio of the second stress invariant on the tensile meridian. Tabs. 4 and 5 provide a summary of the essential characteristics of the concrete used in central columns.

Tension stiffening of concrete		Tension damage in concrete	
Stress/MPa	Cracking strain	d_t	Cracking strain
2.550	0	0	0
2.123	0.000084	0.1104	0.000084
1.398	0.000161	0.2776	0.000161
0.818	0.000302	0.5492	0.000302
0.476	0.000553	0.7920	0.000553
0.318	0.000894	0.9004	0.000894
0.224	0.001397	0.9502	0.001397
0.171	0.002111	0.9701	0.002111
0.141	0.002603	0.9790	0.002603
0.128	0.003005	0.9830	0.003005
0.088	0.005005	0.9850	0.005005

Table 4: Concrete damage plasticity model constitutive parameters (tension).

Compression hardening in concrete		Compression damage in concrete	
Stress/MPa	Crushing strain	d_c	Crushing strain
13.576	0	0	0
27.525	0.00035	0.1154	0.00035
30.120	0.00075	0.2069	0.00075
25.119	0.00163	0.4029	0.00163
15.535	0.00348	0.7074	0.00348
11.592	0.00470	0.8159	0.00470
7.605	0.00629	0.8905	0.00629
5.893	0.00783	0.9273	0.00783
4.798	0.00935	0.9482	0.00935
4.038	0.01085	0.9601	0.01085
3.195	0.01336	0.9721	0.01336

Table 5: Concrete damage plasticity model constitutive parameters (compression).

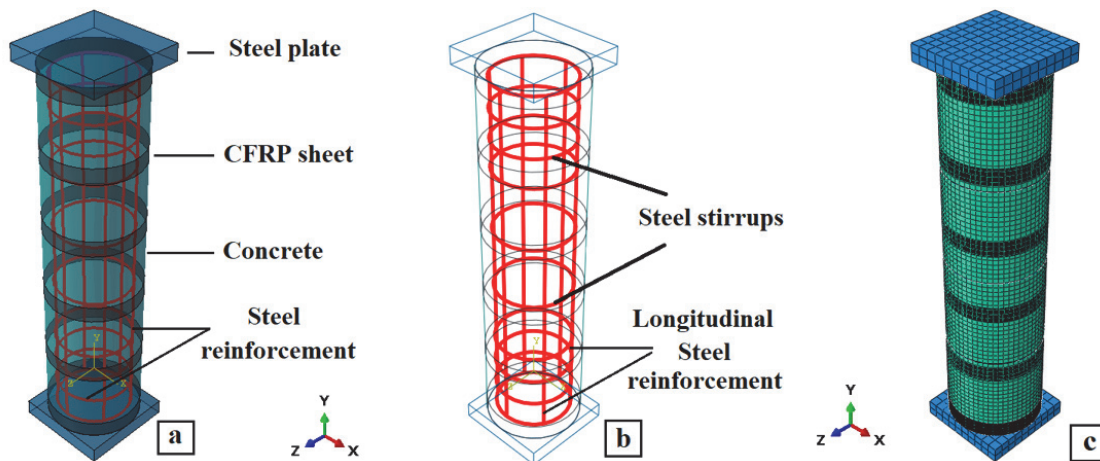Figure 3: (a) Specimen's model, (b) Steel configuration and (c) Specimen's mesh

To match the load-defection curves for theoretical and experimental samples, several attempts were performed. Also, the meshing size of the steel bar, concrete, and CFRP elements were examined. The mesh sizes ranged from 10 to 40 mm with an increment of 5 mm. The best assessment was realized at the mesh size of 20 mm for steel bars and steel plate elements. Also, for concrete and CFRP elements, the selected mesh size was 10 mm. The viscosity parameter values used ranged from

0.0005 to 0.003. It was found that the viscosity parameter value of 0.001 led to close agreement between FEA and experimental results. The dilation angle (ψ) values used ranged from 32 and 44°. The best result occurred when the dilation angle (ψ) value was 40°. For shape factor (k), stress ratio (f_{bo}/f_{co}) and eccentricity, the default values for these parameters were adopted.

A 4-node shell elements is used in model the CFRP [36-42]. The CFRP is considered as a linear elastic material, while Steel is considered as an elastic - perfectly plastic material. Concrete is simulating by means of improved CDP method. This method in the beginning developed by Lubliner et al. [46] and modified by Lee and Fenves [45]. The damage parameters are calculated by taking into account the experimental mechanical properties test carried out in the laboratory by Kaiss et al. [43]. The adopted model that simulates the concrete uniaxial stress-strain curve in the present study based on Lam and Teng (2003a, b) model [47, 48]. According to ACI 4402R-17 [49] the bond between concrete and CFRP is considered perfect bond. Force-controlled loads are used in experimental work [43] and current numerical analyses. The required input parameters in ABAQUS used to define concrete material model are shown in Tab. 6.

Dilation angle, ψ	40
Eccentricity	0.1
f_{bo}/f_{co}	1.16
k	0.6667
Viscosity parameter	0.001
Compressive strain at peak, ε_c	0.0002
Inelastic strain of concrete in compression, ε_{cin}	0.00082 to 0.0033
Cracking strain of concrete in tension ε_{tck}	0.0002

Table 6: Input parameters to define the concrete material model.

To simulate the boundary condition of numerical specimens, an eccentric pin end at base was simulated to allow rotation and pin supports with degree of freedom of $U_x = U_z = 0$ were placed at the top of specimens to allow for vertical movement and rotation. Moreover, in order to simulate the status of experimental loading an eccentric vertical load was applied on top of the columns. Fig. 4 shows the loads, and boundary conditions.
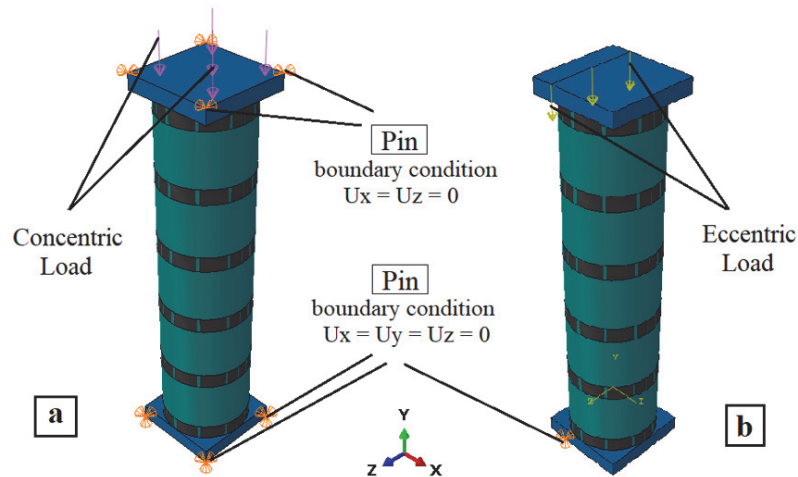

Figure 4: loads and boundary conditions (a) for concentric load and (b) for eccentric load.

PARAMETRIC STUDY

The parametric study presented in this work thorough twenty four numerical circular short column specimens by using finite element ABAQUS software. These specimens were divided into five groups; first group was focused to make validation with experimental work [43], while remain groups focused to investigate the performance of applied load with different eccentricity and ratio of confinement (CFRP ratio %) as shown in Tab. 7. To define specimen IDs presented in Tab. 7, the number subsequent to C letter, represents the specimen's number, subsequently letter A, B, D and E represents the CFRP ratios 0%, 25%, 50%, 100% respectively. The subsequently number represents the eccentricity (e), 0, 10, 20, 30, 40, and 50. For example, C31D0 indicates spacemen number 31, CFRP ratio 50%, and zero eccentricity.

Group No.	Specimen ID	fc' MPa	e mm	CFRP Layers	t_f mm	CFRP ratios %	Remarks
1	C1A0		0	0		0	Validation
	C2B0		0	1		25	Validation
	C3D0		0	1		50	Validation
	C4E0		0	1		100	Validation
2	C5A10		10	0		0	
	C6A20		20	0		0	
	C7A30		30	0		0	
	C8A40		40	0		0	
	C9A50		50	0		0	
3	C10B10		10	1		25	
	C11B20		20	1		25	
	C12B30	30.12	30	1	0.166	25	
	C13B40		40	1		25	
	C14B50		50	1		25	
4	C15D10		10	1		50	
	C16D20		20	1		50	
	C17D30		30	1		50	
	C18D40		40	1		50	
	C19D50		50	1		50	
5	C20E10		10	1		100	
	C21E20		20	1		100	
	C22E30		30	1		100	
	C23E40		40	1		100	
	C24E50		50	1		100	

Table 7: Details of numerical specimens.

RESULTS AND DISCUSSION

C urrent numerical study of eccentrically loaded circular short reinforced concrete columns confined with different CFRP ratio was performed using the improved CDP.

Verification of numerical results

The differences between numerical and experimental data [43] are shown in Tab. 8. The concentric load – longitudinal displacement and concentric load - lateral strain at columns midpoint curves of specimens in group 1 (C1A0, C2B0, C3D0, and C4E0) obtained from the FE analysis along with the experimental data [43] are compared in Fig. 5 and Fig. 6. These figures illustrate that the FE model and the experimental data were good similar. It can be seen that the ratio of the numerical to experimental axial compressive strength ($P_{Num.} / P_{Exp}$), maximum longitudinal displacement ($\Delta_{Num} / \Delta_{Exp}$) and lateral strain ($\epsilon_{Exp} / \epsilon_{Num}$) ranges between (0.91-0.97), (0.98-1.03) and (1.01-1.10) respectively. Figs. 7 show the comparisons between numerical plastic strain and experimental mode of failure [43]. Also, Fig. 7 shows the experimental and numerical damage for verified specimens under concentric load. Tab. 9 summarized the numerical results.

Group No.	Specimen ID	Experimental values of the axial compressive strength (kN)	Numerical values of the axial compressive strength (kN)	P_{Num} / P_{Exp}	Max. Experimental longitudinal displacement (mm)	Max. Numerical longitudinal displacement (mm)	$\Delta_{Num} / \Delta_{Exp}$	Experimental Lateral strain (mm/mm)	Numerical Lateral strain (mm/mm)	$\epsilon_{Exp} / \epsilon_{Num}$
1	C1A0	482	467.6	0.97	5.6	5.66	1.01	0.0011	0.0010	1.10
	C2B0	633	576.2	0.91	4.11	4.12	1.00	0.00245	0.0024	1.02
	C3D0	721	672.1	0.93	4.2	4.12	0.98	0.00353	0.0035	1.01
	C4E0	875	823.7	0.94	3.81	3.92	1.03	0.00295	0.0029	1.02

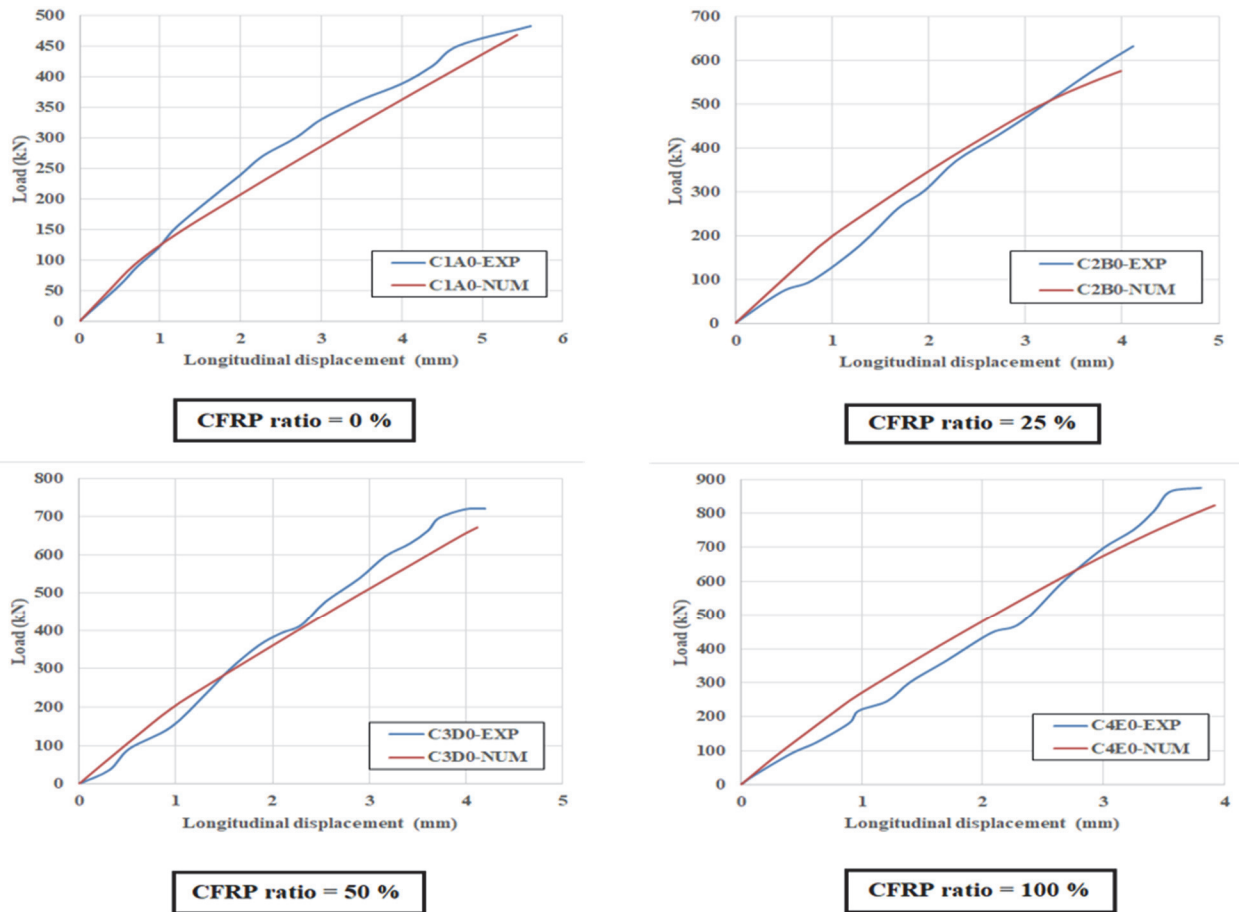Table 8: Comparisons between numerical and experimental results [43].

Figure 5: The experimental and numerical concentric load – longitudinal displacement curves for Group 1.
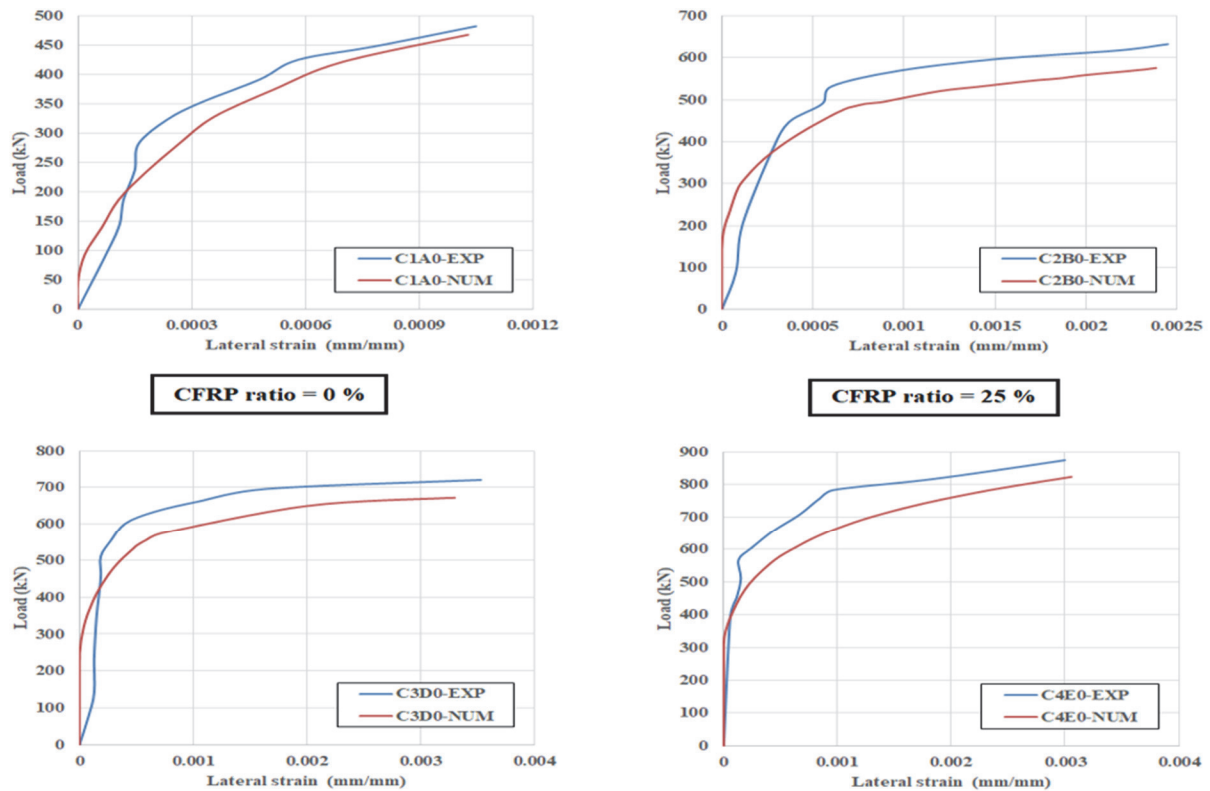

Figure 6: The experimental and numerical concentric load - lateral strain at columns midpoint curves for Group 1.
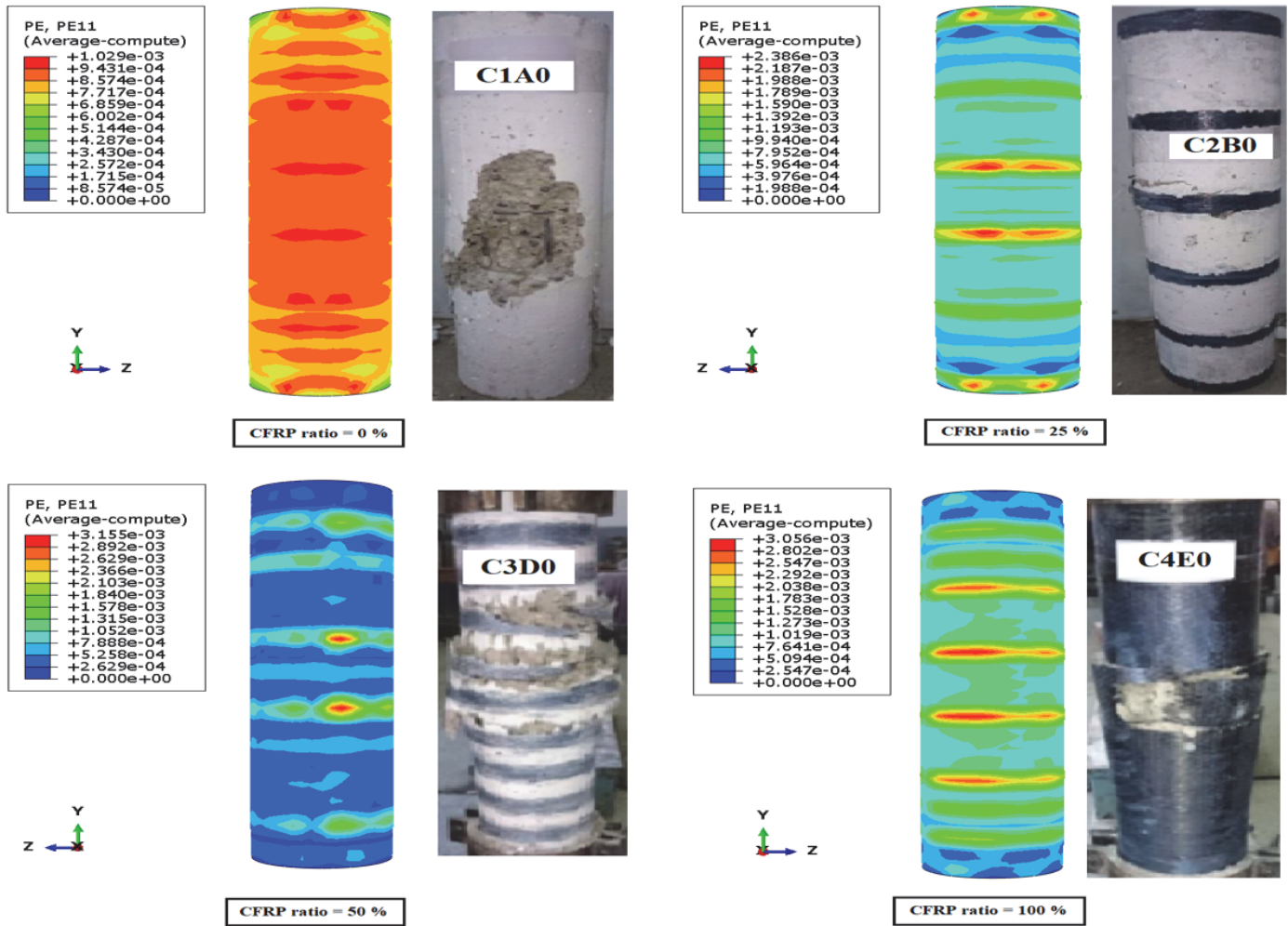
Figure 7: The experimental and numerical damage for verified specimens under concentric load.

Group No.	Specimen ID	Numerical values of the axial compressive strength (kN)	Numerical values of the Deflection (mm)	Lateral strain mm/mm	Decrease in load %	P_{Exp} / P_{Num}	P_{Num} / P_{Exp}
	C5A10	426.24	7.84	0.0013	11.6	1.13	0.885
	C6A20	345.58	10.51	0.0039	28.3	1.39	0.719
2	C7A30	231.25	12.88	0.0057	52.0	2.08	0.481
	C8A40	133.75	15.85	0.0084	72.3	3.60	0.278
	C9A50	83.12	25.95	0.0170	82.8	5.49	0.182
	C10B10	560.55	5.31	0.0041	.114	1.12	0.886
	C11B20	523.49	6.65	0.0056	17.3	1.21	0.827
3	C12B30	490.58	8.39	0.0072	22.5	1.29	0.775
	C13B40	443.73	10.10	0.0089	29.9	1.43	0.700
	C14B50	400.69	11.89	0.0109	36.7	1.58	0.633
	C15D10	656.69	5.11	0.0054	8.9	1.09	0.911
	C16D20	638.04	6.71	0.0083	11.5	1.13	0.885
4	C17D30	601.31	8.07	0.0104	16.6	1.20	0.834
	C18D40	575.36	10.48	0.0142	20.2	1.25	0.798
	C19D50	540.12	13.17	0.0178	25.1	1.33	0.749
	C20E10	797.07	8.63	0.025	8.9	1.09	0.911
	C21E20	783.22	13.88	0.059	10.5	1.11	0.895
5	C22E30	758.99	17.85	0.097	13.3	1.15	0.867
	C23E40	715.27	20.11	0.146	18.3	1.22	0.817
	C24E50	685.27	25.79	0.217	21.7	1.28	0.783

Table 9: Numerical results.

The numerical approach is demonstrated to be capable of accurately forecasting the load carrying capacity, maximum longitudinal displacement, lateral strain and failure mode of the test columns. Since the error in the specimens are within 10%. This result is consistent with Yu et al. [36] findings. This error is caused by effective confining stress used define stress in concrete under non-uniform confinement. Yu et al. [39] calculated this using data from experimental programs done four decades ago.

Effect of Load Eccentricity and CFRP ratio of confinement on Load carrying capacity of columns specimens
To investigate the degradation of axial strength affected by load eccentricity, the factor of strength Ne/Nco is defined and analyzed. Where Ne define as numerical load capacity of column for different CFRP ratio of confinement (CFRP ratio 0%, 25%, 50% and 100%) with or without load eccentricity. Also, Nco is the numerical load capacity for unconfined specimens under concentric load (i.e C1A0). This method of comparing load capacities is widely used in confined concrete analysis [50]. The magnitude of the load eccentricity is represented by the non-dimensional term 2e/D. When Ne/Nco values are compared, it is clear that as the load eccentricity increase the axial strength decreases. This decrement becomes more significant for unconfined specimens (Group 2), as shown in Fig. 8. While when the degree of confinement ratio increases as in Group 3, 4 and 5 the strength increases and the reduction are limited. This agrees with previous finding by Hadi [6].
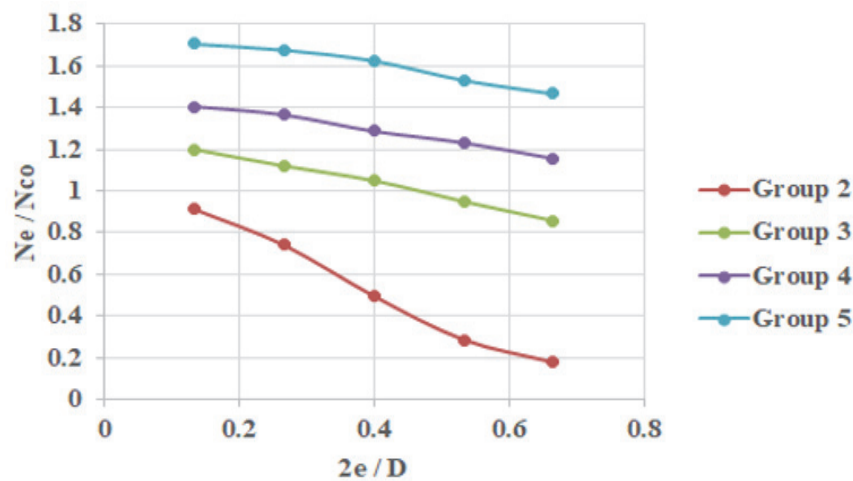

Figure 8: Values of Ne/Nco for each group.

To better understand the strength loss owing to load eccentricity. A further comparison using the factor Ne/Nc will be made by changing the data in Fig. 8. Where Nc define as numerical load capacity of specimens under concentric load with the same ratio of confinement as Ne. Fig. 9 depicts the results. It may be deduced that the load eccentricity-induced degradation of unconfined columns (Group 2). While when the degree of confinement ratio increases as in Group 3, 4 and 5, the axial strength of the specimens is less affected than in unconfined specimens.
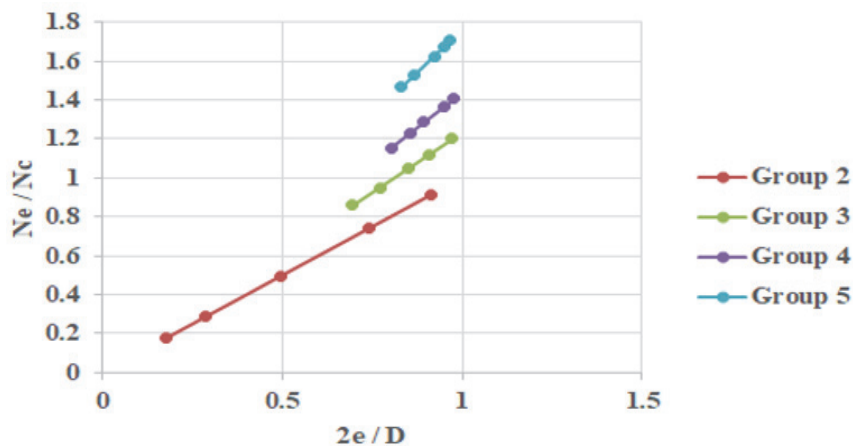

Figure 9: Values of Ne/Nc for each group.

The influence of the load eccentricity on Ne/Nf. Where Nf define as numerical load capacity of unconfined columns specimens with the same eccentricity of load as Ne, can be used to further analyze the contribution of the CFRP confinement ratio. Fig. 10 depicts the comparing results. For the term Ne/Nf, the confinement efficiency can be simply determined. So that because a high value of ratio Ne/Nf indicates an augmentation of strength due to efficiency of CFRP confinement. Fig. 10 show that as load eccentricity increases the Ne/Nf value increases for most CFRP confined circular concrete specimens. However, increasing load eccentricity reduces confinement efficiency, which is understandable given the circular section's lower compressive area. Because the natural axis is so short, large eccentricities exhibit a stronger trend.
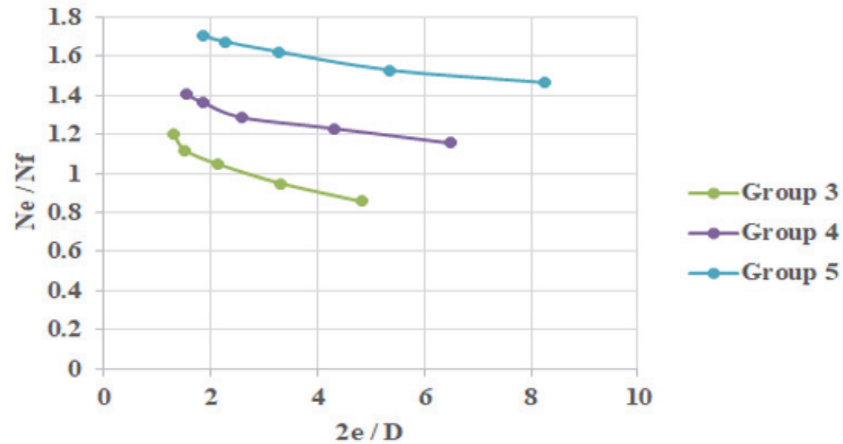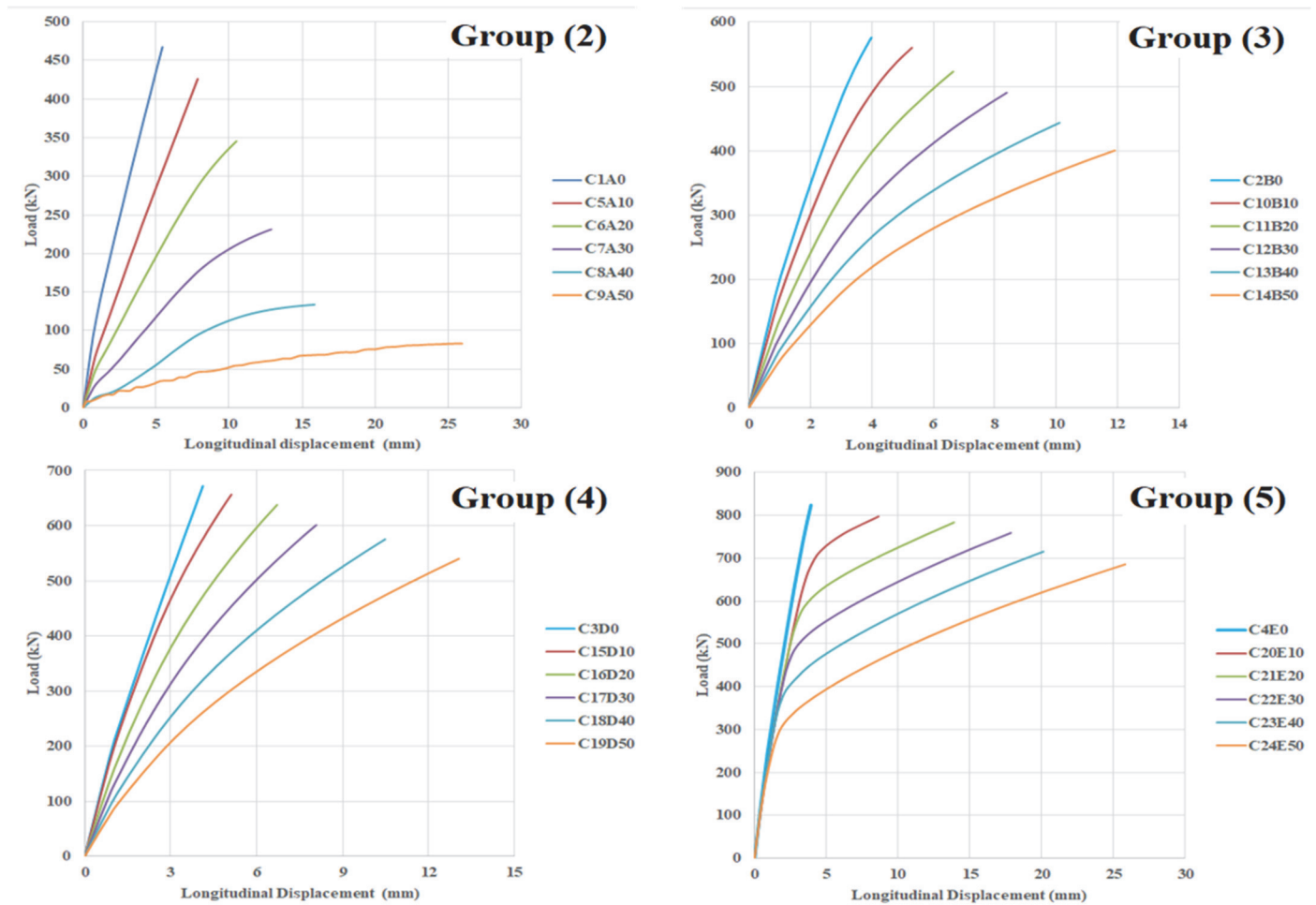

Figure 10: Values of Ne/Nf for each group

Figure 11: The load- longitudinal displacement curves for eccentrically loaded confined columns.

LONGITUDINAL DISPLACEMENT OF COLUMNS SPECIMENS

Fig. 11 depicts the load- longitudinal displacement curves for eccentrically loaded confined columns. It is clear that the columns improved their performance by increasing their displacement at failure (i.e ductility). The ductility of the confined columns increases as the degree of confinement ratio increases (CFRP ratio).

Lateral strain of columns specimens

Fig. 12 show that all of the axial load-lateral strain curves of specimens in the simulated specimens have a bilinear shape with two segments. The first section is linear, and the second section is nonlinear. Also, Fig. 12 shows that as the CFRP ratio increases, so does the ultimate lateral strain. This is due to the fact that increasing the CFRP ratio reduces the clear spacing between adjacent CFRP strips, resulting in an increase in confinement stiffness.
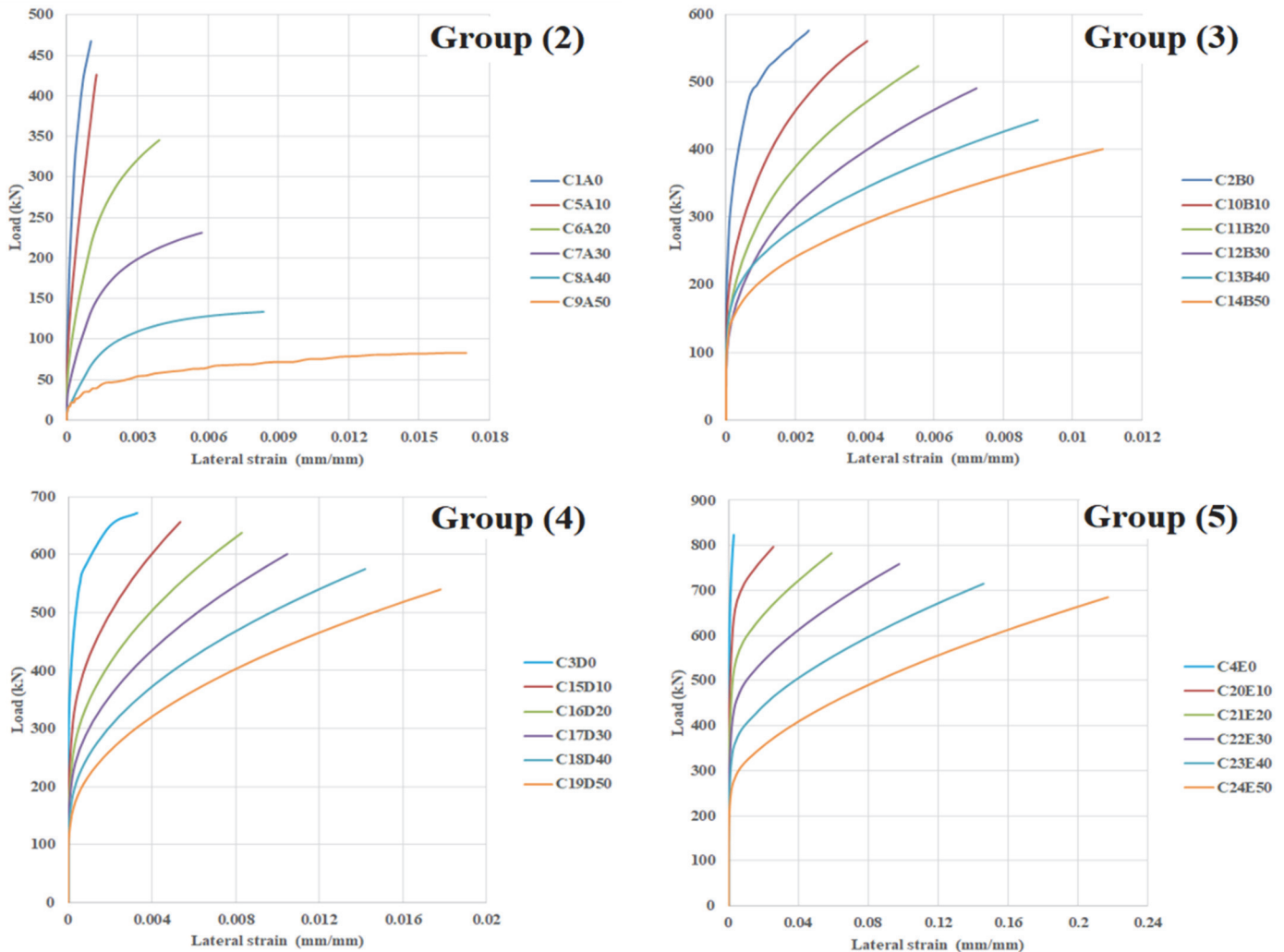

Figure 12: The load- lateral strain curves for eccentrically loaded confined columns.

FAILURE MODE AND CONCRETE PLASTIC STRAIN (DAMAGE)

Fig. 13 depicts the compression failure mode and damage progression obtained using numerical analysis for unconfined specimens under eccentric load. Also, with damage concentration at the concrete cover on the higher compression side at mid height of column specimens due to stress gradient from additional bending loads. While confined columns fail, the CFRP strips rupture, resulting in concrete crushing on the compression side. This is thought to be due to the specimens' clear strip spacing, which caused by localized concrete crushing failure.
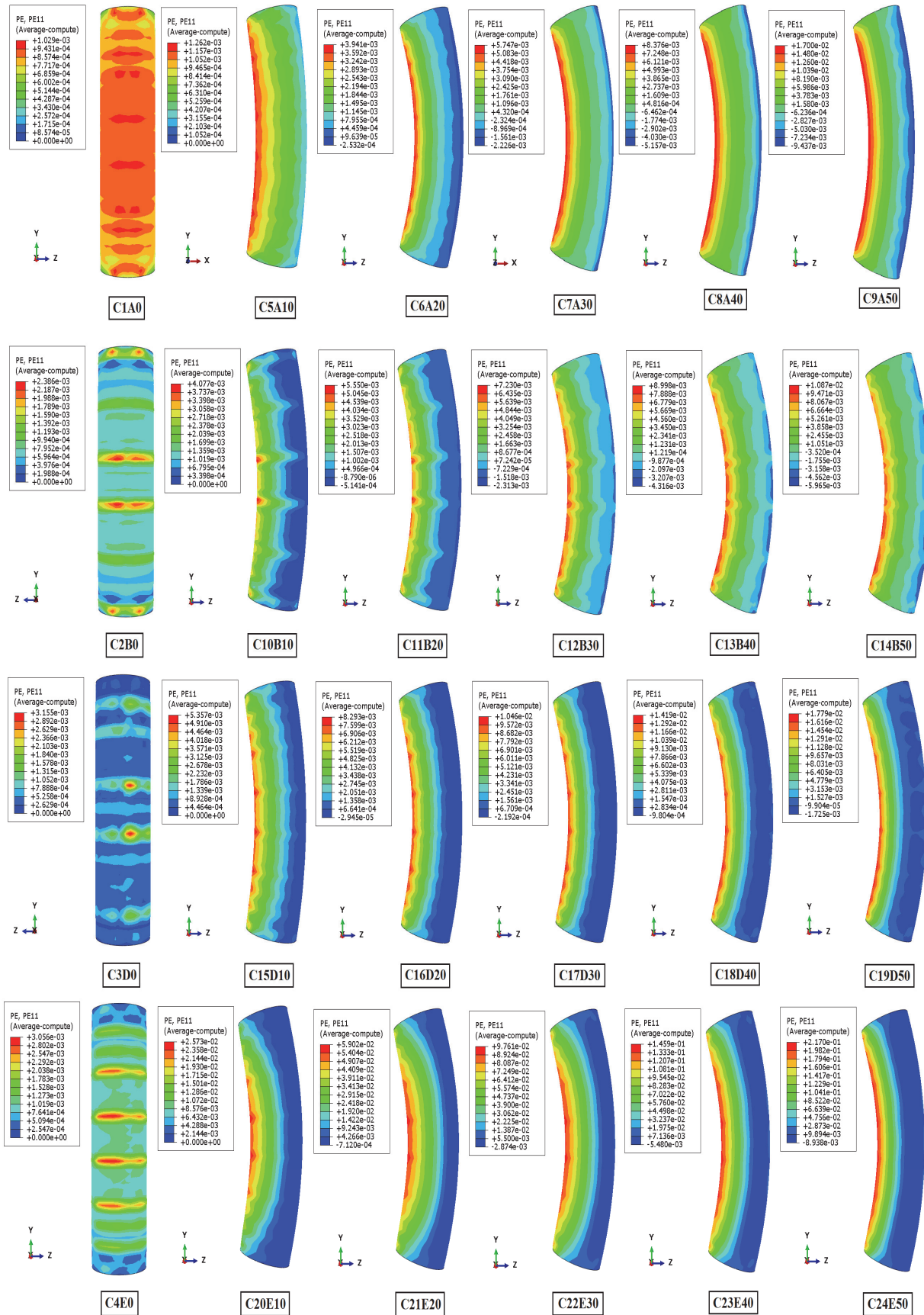
Figure 13: The numerical damage (lateral plastic strain P11) for specimens under eccentric load

CONCLUSIONS

From the outcomes of our investigation to study the effect of load eccentricity and different degrees of confinement ratio of CFRP on the behavior of circular short columns by using improved CDP finite element analysis. The following conclusion can be drawn:

1- The used numerical analytical model validated by using literature-based experimental test findings. Based on the validation results, it can be stated that the experimental and numerical findings are in good similar. The numerical models utilized in this work are appropriate for this type of structure analysis.

2- It is obvious that as load eccentricity increases, axial strength decreases, and the reduction in strength becomes more significant for unconfined specimens. When the degrees of confinement ratio increases, so does the strength, and the reduction is limited.

3- The increase in CFRP confinement ratio will improves column's load-bearing capability under the same level of load eccentricity of unconfined columns.

4- The ultimate longitudinal displacement and ultimate lateral strain both increase significantly as the CFRP confinement ratio increases.

REFERENCES

[1] Madqour, M., Fawzi, K. and Hassan, H. (2021). Finite element modeling of flexural behavior of reinforced concrete beams externally strengthened with CFRP sheets, Frattura ed Integrità Strutturale, 16(59), pp. 62–77. DOI: 10.3221/IGF-ESIS.59.05.

[2] Emara, M., Elkomy, N. and Abdel Kader, H. (2021). Numerical Assessment of Reinforced Concrete Beams Strengthened with CFRP Sheets under Impact Loading, Frattura ed Integrità Strutturale, 15(58), pp. 48–64. DOI: 10.3221/IGF-ESIS.58.04.

[3] Zhu, H. (2018). Stress performance of embedded carbon fiber reinforced plastics plate consolidated reinforced concrete structure, Frattura ed Integrità Strutturale, 12(46), pp. 361–370. DOI: 10.3221/IGF-ESIS.46.33.

[4] Wu, Y. and Jiang, C. (2014), Stress- Strain Model for Eccentrically Loaded FRP- Confined Concrete Columns. In: The International Conference on FRP Composites in Civil Engineering.

[5] Parvin, A. and Wang, W. (2001). Behavior of FRP Jacketed Concrete Columns under Eccentric Loading, Journal of Composites for Construction, 5(3), pp. 146–152.

[6] Li, J. and Hadi, M.N. (2003). Behaviour of externally confined high-strength concrete columns under eccentric loading, Composite Structures, 62(2), pp. 145–153.

[7] Fitzwilliam, J. and Bisby, L. (2006), Slenderness effects on circular FRP wrapped reinforced concrete columns. In: Third International Conference on FRP Composites in Civil Engineering. .

[8] Yung, Wang, C. and Restrepo, J. (2001). Investigation of Concentrically Loaded Reinforced Concrete Columns Confined with Glass Fiber-Reinforced Polymer Jackets, ACI Structural Journal, 92(3), pp. 144–157.

[9] El Maaddawy, T. (2009). Strengthening of eccentrically loaded reinforced concrete columns with fiber-reinforced polymer wrapping system: Experimental investigation and analytical modeling, J. Compos. Constr. 13, pp. 13–24.

[10] Chellapandian, S.S., Prakash, A. and Rajagopal. (2018). Analytical and finite element studies on hybrid FRP strengthened RC column elements under axial and eccentric compression, Composite Structures, 184, pp. 234–248.

[11] Wu, Y.F. and Jiang, C. (2013). Effect of load eccentricity on the stress-strain relationship of FRP-confined concrete columns, Compos. Struct, 98, pp. 228–241.

[12] Lin, G. and Teng, J.G. (2017). Three-dimensional finite-element analysis of FRP-confined circular concrete columns under eccentric loading, J. Compos. Constr, 21, pp. 4017003–4017003.

[13] Lorenzis, L. and Tepfers, R. (2003). Comparative study of models on confinement of concrete cylinders with fiber-reinforced polymer composites, J. Compos. Constr, 7, pp. 219–237.

[14] Choi, E., Kim, J.W., Rhee, I. and Kang, J.W. (2014). Behavior and modeling of confined concrete cylinders in axial compression using FRP rings, Compos. B Eng, 58, pp. 175–184.

[15] Fam, A., Flisak, B. and Rizkalla, S. (2003). Experimental and analytical modeling of concrete-filled fiber-reinforced polymer tubes subjected to combined bending and axial loads, ACI Struct. J, 100, pp. 499–509.

[16] Tao, Z., Teng, J.G., Han, L.H. and Lam, L. (2004). Experimental behaviour of FRP-confined slender RC columns under eccentric loading. In: Proceedings of the 2nd International Conference on Advanced Polymer Composites for Structural Applications in Construction. pp. 203–212.

[17] Hadi, M.N.S. (2006). Comparative study of eccentrically loaded FRP wrapped columns, Compos. Struct, 74, pp. 127–135.

[18] Hadi, M.N. (2006). Behaviour of FRP wrapped normal strength concrete columns under eccentric loading, Compos. Struct, 72, pp. 503–511.

[19] Hadi, M.N. (2007). Behaviour of FRP strengthened concrete columns under eccentric compression loading, Compos. Struct, 77, pp. 92–96.

[20] Hadi, M.N.S. (2007). The behaviour of FRP wrapped HSC columns under different eccentric loads, Compos. Struct, 78, pp. 560–566.

[21] Hadi, M.N.S. (2009). Behaviour of eccentric loading of FRP confined fibre steel reinforced concrete columns, Constr. Build. Mater, 23, pp. 1102–1108.

[22] Bisby, L. and Ranger, M. (2010). Axial-flexural interaction in circular FRP-confined reinforced concrete columns, Constr. Build. Mater, 24, pp. 1672–1681.

[23] Cao, Y., Wu, Y.F. and Jiang, C. (2018). Stress-strain relationship of FRP confined concrete columns under combined axial load and bending moment, Compos. Part B Eng, 134, pp. 207–217.

[24] 21. Chaallal, O. (2000). Shahawy, M. Performance of fiber-reinforced polymer-wrapped reinforced concrete column under combined axial-flexural loading, ACI Struct. J, 97, pp. 659–668.

[25] Maaddawy, T. (2008). Behavior of corrosion-damaged RC columns wrapped with FRP under combined flexural and axial loading, Cem. Concr. Compos, 30, pp. 524–534.

[26] El Maaddawy, T. (2008). Post-repair performance of eccentrically loaded RC columns wrapped with CFRP composites, Cem. Concr. Compos, 30, pp. 822–830.

[27] Elwan, S.K. and Rashed, A.S. (2011). Experimental behavior of eccentrically loaded R.C. short columns strengthened using GFRP wrapping, Struct. Eng. Mech, 39, pp. 207–221.

[28] Hadi, M.N.S. and Widiarsa, I.B.R. (2012). Axial and flexural performance of square RC columns wrapped with CFRP under eccentric loading, J. Compos. Constr, 16, pp. 640–649.

[29] Hajsadeghi, M. and Alaee, F. (2010). Numerical analysis of rectangular reinforced concrete columns confined with FRP jacket under eccentric loading, The 5th International Conference on FRP Composites in Civil Engineering, Beijing, China, pp. 658–661.

[30] Quiertant, M. and Clement, J. (2011). Behavior of RC columns strengthened with different CFRP systems under eccentric loading, Constr. Build. Mater, 25, pp. 452–460.

[31] Sadeghian, P., Rahai, A.R. and Ehsani, M.R. (2010). Experimental study of rectangular RC columns strengthened with CFRP composites under eccentric loading, J. Compos. Constr, 14, pp. 443–450.

[32] Shaheen, E. and Shrive, N.G. (2007). Sprayed glass fibre reinforced polymer masonry columns under concentric and eccentric loading, Can. J. Civ. Eng, 34, pp. 1495–1505.

[33] Liu, Y., Dong, A., Zhao, S., Zeng, Y. and Wang, Z. (2021). The effect of CFRP-shear strengthening on existing circular RC columns under impact loads. Construction and Building Materials, 302, 124185.

[34] Liu, X., Zheng, Y.Z., Fang, Q., Zhou, C., Yang, Y., Xiang, H.B. and Yan, H.C. (2022). Anti-collision performance of RC columns strengthened with a composite of FRP grid and UHPC. Structures, 43, pp. 1682-1691.

[35] Al-Rousan, R. (2020). Behavior of circular reinforced concrete columns confined with CFRP composites. Procedia Manufacturing. 44, pp.623-30.

[36] Yu, T., Teng, J.G., Wong, Y.L. and Dong, S.L. (2010). Finite element modeling of confined concrete-II: Plastic-damage model, Eng. Struct. (32), pp. 680–691.

[37] Parvin, A. and Schroeder, J. (2008). Investigation of eccentrically loaded CFRP-confined elliptical concrete columns, J. Compos. Constr, 12, pp. 93–101.

[38] Hu, B., Wang, J.G. and Li, G.Q. (2011). Numerical simulation and strength models of FRP-wrapped reinforced concrete columns under eccentric loading, Constr. Build. Mater, 25, pp. 2751–2763.

[39] Yu, T., Teng, J.G., Wong, Y.L. and Dong, S.L. (2010). Finite element modeling of confined concrete-I: Drucker-Prager type plasticity model, Eng. Struct, 32, pp. 665–679.

[40] Jiang, J.F. and Wu, Y.F. (2014). Characterization of yield surfaces for FRP-confined concrete, J. Eng. Mech, pp. 4014096–4014096.

[41] Mazzucco, G., Salomoni, V., Majorana, C., Pellegrino, C. and Ceccato, C. (2016). Numerical investigation of concrete columns with external FRP jackets subjected to axial loads, Constr. Build. Mater, 111, pp. 590–599.

[42] Teng, J.G., Xiao, Q.G., Yu, T. and Lam, L. (2015). Three-dimensional finite element analysis of reinforced concrete columns with FRP and/or steel confinement, Eng. Struct. (97), pp. 15–28.

[43] Kaiss, S., Raid, K. and Mohammed, H. (2018). Influence of ties on the behavior of short reinforced concrete columns strengthened by external CFRP, MATEC Web of Conferences, 162, pp. 4005–4005.

[44] (2008). ABAQUS theory manual, user manual and example manual, Version 6, vol. 8. Providence, RI: Karlsson & Sorensen Inc.

[45] Lee, J. and Fenves, G.L. (1998). Plastic-damage model for cyclic loading of concrete structures, J Eng Mech, 124.

[46] Lubliner, J., Oliver, J., Oller, S. and On ate, E. (1989). A plastic damage model for concrete, Int J Solids Struct, 25, pp. 299-326.

[47] Lam, L. and Teng, J. (2003). Design-Oriented Stress-Strain Model for FRP-Confined Concrete, construction & building materials, 17(6-7), pp. 471-489.

[48] Lam, L. and Teng, J. (2003). Design-Oriented Stress-Strain Model for FRP-Confined Concrete in Rectangular Columns, Journal of Reinforced Plastics and Composites, 22(13), pp. 1149-1186.

[49] (2017). Design and Construction of Externally Bonded FRP Systems for Strengthening Concrete Structures (ACI 440.2R-17), vol. 112. Farmington Hills, MI: American Concrete Institute.

[50] Wei, Y., Jiang, C. and Wu, Y.F. (2019). Confinement effectiveness of circular concrete-filled steel tubular columns under axial compression, Journal of Constriction and Steel Research, 158, pp. 15–27.